Model-Based Interpretation of Measurements for Fatigue Evaluation of Existing Reinforced Concrete Bridges

Imane Bayane[1]; Sai G. S. Pai[2]; Ian F. C. Smith, F.ASCE[3]; and Eugen Brühwiler[4]

Abstract: New methods are required for sustainable and economical management of bridges. Efficient management can be achieved by a detailed understanding of bridge behavior through monitoring and model-based data interpretation. This paper presents a methodology to evaluate the fatigue safety of existing bridges based on conducting measurements onsite and interpreting measurement data using physics-based behavior models. The methodology combines data from different nondestructive measurements with structural models to develop a suitable set of feasible models that describe accurately structural behavior. The methodology is illustrated with a case study of a composite steel–concrete road viaduct instrumented with acoustic emission channels and strain gauges. Information from measurements is used to update a set of structural models and then evaluate the fatigue safety of the viaduct. While commonly used *curve-fitting* methods are inaccurate, this methodology is useful to accurately employ the measured behavior of existing civil infrastructure for evaluating nonaccessible elements and scheduling inspections and decision-making related to actions such as strengthening and retrofit. **DOI: 10.1061/(ASCE)BE.1943-5592.0001742**. *This work is made available under the terms of the Creative Commons Attribution 4.0 International license, https://creativecommons.org/licenses/by/4.0/.*

Author keywords: Bridge; Structural identification; Acoustic emission; Nondestructive testing; Load test; Numerical model; Error-domain model falsification; Residual minimization.

Downloaded from ascelibrary.org by 92.106.24.211 on 06/25/21. Copyright ASCE. For personal use only; all rights reserved.

Introduction

With an increasing demand for infrastructure management, challenges exist in managing the stock of structures while building new ones. Bridge management is particularly challenging due to the large stock of bridges that have to be evaluated at a state level (Mauro 2017). Reliable methods of evaluation are therefore necessary to allocate resources to the maintenance of bridges to ensure their utility over their lifetimes at a reasonable cost.

Monitoring and nondestructive testing (NDT) can provide valuable information about the current condition of bridges. In the last few decades, many monitoring and testing techniques have been developed to improve knowledge of structural response. For example, techniques involving optic-fiber sensing, radiography, ground-penetrating radar, image correlation, tomography, ultrasonication, and acoustic emission (AE) have been proposed (Breysse 2012a; Maierhofer et al. 2010; Méndez and Csipkes 2013). However, a close examination of the previous work reveals the important challenge of transforming measurement data into knowledge that is helpful for structural identification and useful for decision-making.

The large size of civil infrastructure elements and the changing environments to which they are exposed create challenges for many techniques that otherwise fare well in laboratory settings (Farrar and Worden 2010; Breysse 2012b; Nguyen et al. 2013). Furthermore, the monitoring and testing techniques are limited to accessible structural components and they cannot be used for instrumenting a whole structure to obtain direct measurements. Moreover, collected data are often interpreted qualitatively, and the effect of uncertainties related to measurement error and bias are not quantified during measurement interpretation, which make measurement data not useful for decision-making. Therefore, appropriate physics-based models and engineering expertise are required to interpret measurements and evaluate concrete bridges.

To overcome limitations related to site implementation, techniques are chosen in this research based on their capacity for long-term monitoring with an occasional onsite inspection that does not interrupt the operational use of a structure or cause damage. The AE technique is used to investigate structural behavior under traffic and environmental actions. AE involves the study of elastic waves generated during a stress-state change in material to understand the physical and mechanical condition of the propagation zone (Beattie 2013). The technique has been widely used to assess concrete bridges during load tests (Felux 2017; Anay et al. 2016; Golaski et al. 2002). In addition, sound velocity measurement and rebound-hammer testing are performed for concrete-strength assessment onsite. Finally, strain and deflection measurements are conducted to evaluate the mechanical response of the structure under a load test and normal traffic.

[1]Doctoral Assistant, Laboratory for Maintenance and Safety of Structures, School of Architecture, Civil and Environmental Engineering, Swiss Federal Institute of Technology (EPFL), Lausanne 1015, Switzerland (corresponding author). ORCID: https://orcid.org/0000-0002-0928-9790. Email: imane.bayane@epfl.ch

[2]Postdoctoral Researcher and Project Coordinator, Cyber Civil Infrastructure, Future Cities Laboratory, Singapore-ETH Centre, ETH-Zurich, Singapore 138602. Email: sai.pai@sec.ethz.ch

[3]Principal Investigator, Cyber Civil Infrastructure, Future Cities Laboratory, Singapore-ETH Centre, ETH-Zurich, Singapore 138602; Professor and Head of Laboratory, Applied Computing and Mechanics Laboratory, School of Architecture, Civil and Environmental Engineering, Swiss Federal Institute of Technology (EPFL), Lausanne 1015, Switzerland. Email: ian.smith@epfl.ch

[4]Professor and Head of Laboratory, Laboratory for Maintenance and Safety of Structures, School of Architecture, Civil and Environmental Engineering, Swiss Federal Institute of Technology (EPFL), Lausanne 1015, Switzerland. Email: eugen.bruhwiler@epfl.ch

Note. This manuscript was submitted on August 14, 2020; approved on March 17, 2021; published online on June 3, 2021. Discussion period open until November 3, 2021; separate discussions must be submitted for individual papers. This paper is part of the ***Journal of Bridge Engineering***, © ASCE, ISSN 1084-0702.

To consider the potential impact of uncertainties during measurement interpretation and provide quantitative information on the structure's behavior at nonaccessible locations, information from measurements is combined with physics-based models. Interpreting measurement data using physics-based models has been referred to as structural identification, model calibration, and model updating (Farrar and Worden 2010). It is an ill-posed inverse task that is sensitive to incomplete knowledge of uncertainties, systematic bias, and correlations between uncertainties at measurement locations (Goulet and Smith 2013).

Error-domain model falsification (EDMF) and residual minimization (RM) are used for structural identification. RM is widely used in practice to calibrate structural models and it is computationally inexpensive. However, it does not consider measurement and model uncertainty and bias. While EDMF is one of the structural-identification methodologies that has been successfully applied to more than 20 full-scale data-interpretation challenges (Goulet and Smith 2013; Pasquier et al. 2014; Smith 2016; Pai et al. 2018). EDMF has been shown to provide more accurate structural identification compared with other methodologies such as RM and traditional Bayesian model updating. Comparisons of these methodologies have been made on many full-scale case studies (Pai et al. 2018; Pasquier et al. 2014; Smith 2016) as well as in theoretical examples where the *ground truth* is known. Finally, no work has combined AE results with advanced structural identification methods.

This paper presents an approach to interpret AE and strain measurements onsite using physics-based models calibrated using EDMF and RM, with the aim to evaluate accurately the fatigue safety of nonaccessible elements. The approach is illustrated through a case study of a reinforced concrete (RC) bridge deck slab currently in service. The next section describes the measurement techniques, the structural identification methods, and the requirements used for fatigue safety evaluation. In the section "Measurements," measurement results are presented and discussed. In the section "Model-Based Data Interpretation," the development of structural models for data interpretation is described. In section "Fatigue Evaluation," the use of the validated models is illustrated for fatigue evaluation of nonaccessible elements. The objectives of this work are as follows:

- O1. Evaluating the use of AE for developing physics-based models and for structural identification of existing bridges.
- O2. Comparing and validating solutions for structural identification obtained using EDMF and RM to predict accurate responses at nonaccessible locations.
- O3. Assessing fatigue safety using validated knowledge of structural behavior obtained by interpreting measurements with a physics-based model.
- O4. Demonstrating with a full-scale case study the utility of monitoring to support bridge management decisions.

Methodology

Rebound-Hammer Testing

The rebound hammer is an NDT that provides information related to the compressive strength of concrete. After every impact, the rebound value is saved and an average value of 10 rebound values is calculated and compared with measured values. Values that are greater or less than 10% of the average value are not included and the average is recalculated. The compressive strength of concrete is obtained using the conversion curve that can be found in the user manual (Proceq SA 2017) considering the rebound value and the impact direction. The median of compressive strength values is calculated based on requirements of the standard (NF EN 12504-2, AFNOR 2013). Young's modulus of concrete is then estimated from the characteristic strength according to Eq. (5). 1–20 of the recommendations of the International Federation for Structural Concrete (FIB) (fib 2010).

Sound Velocity Measurement

Sound velocity measurement is an NDT used to assess the compressive strength of materials. The test is carried out by passing elastic waves through materials and measuring the time of propagation to calculate wave velocity. The velocity of an elastic wave propagating through a medium depends on elastic constants and the mass density of the material. Elastic waves are comprised of compression or *P*-waves (first arrivals of a wave) and shear or *S*-waves (second arrivals of a wave).

The velocities of *P* waves v_p and *S* waves v_s are related to Young's modulus E, Poisson's ratio υ, and density ρ of the environment according to the following equations:

$$v_p = \sqrt{\frac{E(1-\upsilon)}{\rho(1+\upsilon)(1-2\upsilon)}} \tag{1}$$

$$v_s = \sqrt{\frac{E}{2\rho(1+\upsilon)}} \tag{2}$$

Understanding the velocity of these waves provides information about the internal condition of the environment through which the waves propagate.

Acoustic Emission

The AE technique involves the study of elastic waves generated during a stress-state change in material to understand the physical state of the propagation zone (Beattie 2013). The stress change is assumed to be rapid enough to transmit the energy and dissipate it as an elastic wave. AE involves the use of sensors that detect elastic waves and convert them into electrical signals. The recorded signals are collected, preprocessed, and stored in a data acquisition system, where it is possible to extract, process, and visualize recorded data (Nair and Cai 2010). AE data can be processed through many approaches, of which the most important are the parameter-based analysis (Aggelis 2011; Felux 2017; Nair and Cai 2010) and the *b*-value analysis (Carpinteri et al. 2009; Colombo et al. 2003; Xu et al. 2013).

Parametric-Based Analysis

The parametric-based analysis examines changes in AE features over time. AE feature extraction and analysis are performed using MATLAB (R2019b) and the AEwin for Sensor Highway III program (commercial software for AE feature and waveform processing). Six features are extracted from the recorded waves, as shown in Fig. 1, and are used to perform the analysis: amplitude, duration, counts to peak (Pcounts), absolute energy (ABSenergy), average frequency (AF), and initiation frequency (Ifrequency).

The AE features are defined according to Mistras (2015) as follows:

- Amplitude is the highest voltage in the AE waveform expressed in decibels (dB) (Fig. 1).
- Duration is the time from first to last threshold crossing expressed in microseconds (μs) (Fig. 1).
- Counts to the peak are the number of threshold crossings from first to highest voltage point on the waveform (Fig. 1).

Downloaded from ascelibrary.org by 92.106.24.211 on 06/25/21. Copyright ASCE. For personal use only; all rights reserved.

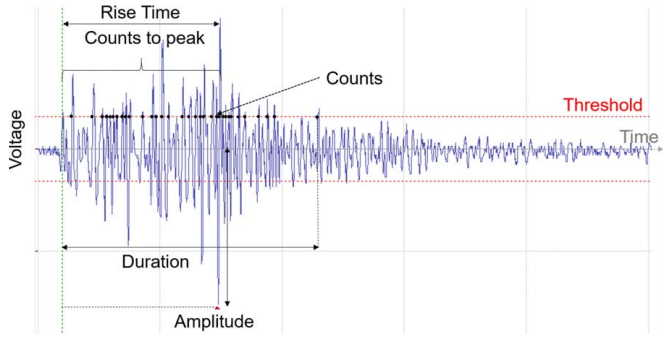

Fig. 1. Acoustic emission features.

- ABSenergy is the time integral of the square of the signal voltage at the sensor before any amplification divided by 10 kΩ impedance and expressed in attojoules (aJ) (1 aJ = 10^{-18} J).
- AF is equal to counts divided by duration expressed in kHz [Eq. (3)].

$$\text{Average frequency} = \frac{\text{Counts}}{\text{Duration}} \tag{3}$$

- Ifrequency is equal to Pcounts divided by rise time expressed in kHz [Eq. (4)].

$$\text{Initiation frequency} = \frac{\text{Counts to peak}}{\text{Rise time}} \tag{4}$$

The terms channel and hit are used as defined in the following:

- Channel is a single AE sensor and the related equipment components for transmitting, conditioning, detecting, and measuring the signals that come from it.
- Hit is the process of detecting and measuring an AE signal on a channel.

Ib-Value Analysis

The *Ib*-value analysis is a statistical method used to evaluate the amplitude–frequency distribution of AE hits (Shiotani 2001). The parameter, *Ib*-value, an improvement of the *b*-value established by Gutenberg–Richter to quantify the succession of many AE hits of low amplitude generated by microcracks and the succession of a few AE hits of high-amplitude hits generated by macrocracks (Whitehurst 1966). The *Ib*-value is a parameter that is used to estimate cracking activity and cracking process based on AE peak amplitude distribution. The formula for *Ib*-value is given as follows:

$$Ib = \frac{\log N(\mu - \alpha_1\sigma) - \log N(\mu - \alpha_2\sigma)}{(\alpha_1 + \alpha_2)\sigma} \tag{5}$$

where *Ib*-value = improved *b*-value (*Ib*-value); log *N* = cumulative frequency of amplitude; μ = mean value of amplitude; σ = standard deviation of amplitude; α_1 = coefficient setting the lower value of amplitude; and α_2 = coefficient setting the upper value of amplitude. The *Ib*-value is multiplied by a coefficient of 20 to compare it to *b*-value giving the quantitative analysis of Colombo et al. (2003) and Sammonds et al. (1994) presented in Table 1.

Load Test

The structural response of the viaduct is evaluated based on the results of a load test performed using a five-axle truck with a legal limit load of 400 kN. The five axles are separately weighted, and their surface of action is identified. Two passages are performed at the midspan of Span 4 with a velocity of 10 km/h and a stop of 10 min to capture both the dynamic and static effect of vehicles. During the load test, deflection and strain variations have been measured continuously.

Table 1. Quantitative result analysis

b-Value	Description
[1, 1.2]	The sensor is very near to a large crack or macrocracks are forming
[1.2, 1.7]	Cracks are uniformly distributed, and macrocracks are stable
>1.7	Microcracks are dominant or macrocracks are opening

Source: Data from Colombo et al. (2003) and Sammonds et al. (1994).

Error-Domain Model Falsification

EDMF is a data-interpretation methodology based on the assertion that models should not be validated by data (weak science); data should be used to falsify models (strong science) (Popper 2005; Goulet and Smith 2013). EDMF has been used in structural identification for different contexts such as leak detection (Moser et al. 2018), fatigue-life evaluation (Pai et al. 2018; Pasquier et al. 2014, 2016), damage evaluation (Reuland et al. 2019a, b), and ultimate-limit state verification (Proverbio et al. 2018; Vernay et al. 2018).

Civil engineering structures are generally designed using conservative and simplified models. Models include significant uncertainties due to approximations and assumptions that can be estimated using engineering heuristics. Examples of such approximations and assumptions are simplifications related to loading conditions, geometrical property definitions, and modeling of boundary conditions, which contribute to modeling uncertainties.

EDMF falsifies models (instances) that provide responses (predictions) that are incompatible with measurements (observations). The criteria for compatibility are defined by considering uncertainties from different modeling and measurement sources. The quantification of many of these uncertainties for full-scale applications requires engineering knowledge.

Starting with feasible ranges of important parameters, an initial model set (IMS) is generated through sampling. Measurements and uncertainty information are then used to falsify (refute) models in the IMS to obtain a candidate model set (CMS) of models that explain measured behavior. Several model classes can be potential candidates to describe the behavior of a system. The model classes take system properties as arguments ($\theta_{i\in[1,n_p]}$), such as geometry, material characteristics, boundary conditions, and loading. The combination of model class (g) and input-parameter set θ gives predictions at each measurement location $i \in [1, n_p]$.

The true response of a system Q_i is approximated by model predictions g_{ki} with modeling error $\varepsilon^*_{\text{model},ki}$ at each measurement location i. Similarly, the true response is observed by measurements y_i with measurement error $\varepsilon^*_{\text{measure},i}$. This can be summarized in the following equation:

$$g_{ki}(\theta^*_k) + \varepsilon^*_{\text{model},ki} = Q_i = y_i + \varepsilon^*_{\text{measure},i} \tag{6}$$

Sources of modeling uncertainties include material properties, geometrical properties, mesh refinement, boundary conditions, the slab–girder connection, and other model simplifications. The uncertainties are estimated using engineering judgment. Sources of measurement uncertainties include the resolution of sensors, position, load, and human error. These uncertainties are estimated based on information from the sensor manufacturer and repeated testing. Uncertainties from model and measurement sources are combined to determine the combined uncertainty, $U_{c,i}$.

Downloaded from ascelibrary.org by 92.106.24.211 on 06/25/21. Copyright ASCE. For personal use only; all rights reserved.

Using this combined uncertainty, $U_{c,i}$, the criteria for falsification is determined. The criteria for falsification in EDMF are thresholds computed for target reliability of identification, Φ. This target reliability of identification for civil engineering applications is typically set to 95% ($\Phi = 0.95$). The threshold bounds for falsification, T_{low} and T_{high}, are calculated using the target reliability of identification. Threshold bounds are obtained as follows:

$$\forall\, i \in \{1,\ \ldots,\ n_m\},\ \left\{T_{\text{low},i},\ T_{\text{high},i}\colon \Phi^{1/n_m} = \int_{T_{\text{low},i}}^{T_{\text{high},i}} f_{U_{c,i}}(U_{c,i})dU_{c,i}\right\} \tag{7}$$

where $f_{U_{c,i}}$ = probabilistic distribution function of combined uncertainties at measurement location i. Instances of the model (g) are falsified when model predictions are incompatible with measurements at any sensor location. This compatibility is evaluated using the following equation:

$$\forall\, i\ \in [1,\ \ldots,\ n_m]\colon T_{\text{low},i} \le g_i(\theta) - y_i \le T_{\text{high},i} \tag{8}$$

Model instances that are not falsified form the CMS. These are model instances that demonstrate structural behavior compatible with observations while accounting for uncertainties from modeling and measurement sources. These model instances may be utilized to predict the structural response of nonaccessible elements under conditions that are different from those during sensing to support asset management.

Residual Minimization

RM is commonly used in practice and is computationally inexpensive. It involves the assumption that the difference between model predictions and measurements is governed by the choice of parameters (Mottershead et al. 2011) and that these parameters have zero-mean uncertainty distributions (Smith 2016). The calibration is therefore done by determining the model parameter values that minimize the error between simulation results and measurement data (Sorenson 1970). The objective function for RM is shown in the following equation:

$$\hat{\theta} = \arg\min_{\theta} \sum_{i=1}^{n_y} \left(\frac{g_i(\theta) - \hat{y}_i}{\hat{y}_i}\right)^2 \tag{9}$$

where $\hat{\theta}$ = optimum model parameter set obtained using measurements; $g_i(\theta) - \hat{y}_i$ = residual obtained between the model response $g_i(\theta)$ and measurement $\hat{y}_i$ at location i; and n_y = number of measurement locations. The calibration is therefore done by determining the model parameter values $\hat{\theta}$ that minimize the error between the model response $g_i(\theta)$ and measurement $\hat{y}_i$ for each measurement location $i \in \{1, n_y\}$.

Fatigue Evaluation

Fatigue safety is evaluated according to Swiss code for existing structures SIA 269 (SIA 2013b) following two levels. First, the endurance limit is verified, i.e., the maximum value of the measured stress range must be smaller than the endurance limit of the rebar fatigue detail. If Level 1 of verification is inconclusive, damage accumulation according to Palmgren–Miner's rule is calculated using the recorded histograms of stress cycles and the appropriate S–N curve for the rebar fatigue detail that can be found in (SIA 262:2013, SIA 2013a; SIA 269:2013, SIA 2013b).

Summary of Methodology

The presented methodology for the evaluation of the fatigue behavior of RC bridges is summarized in the following principal steps:

- Estimate material properties using AE and NDT.
- Develop and parametrize physics-based models using AE.
- Update the models using load-test results and EDMF.
- Validate model-updating solutions by comparing updated model predictions with measurements not included for structural identification.
- Predict structural response at nonaccessible locations to evaluate fatigue behavior.

Measurements

Case Study

Monitoring and NDT are performed on an eight-span composite concrete–steel viaduct. It has seven articulated spans of 25.58 m and an approach span of 15.8 m. Each span comprises an RC slab of a thickness varying from 0.17 to 0.24 m connected to two 1.3-m-height steel girder beams.

The viaduct is instrumented with AE channels, strain gauges, and thermocouples for continuous monitoring. Linear variable differential transformers (LVDTs), rebound-hammer testing, and sound–velocity measurement are used for occasional inspections. Fig. 2 illustrates the view of the viaduct and the instrumented span.

AE channels are mounted on the RC slab at midspan, midlane, between midspan and articulation, and between articulation and support of Span 4. Strain gauges are embedded in longitudinal and transverse rebars at midspan and the girder of Span 4. LVDTs are mounted in the middle of Span 4 at five locations (lower flange of the girder, midlane, and midspan). Fig. 3 illustrates the instrumented slab and sensor placement. Rebound-hammer testing and sound–velocity measurement are performed on the lower side of Span 4.

The load test and deflection measurements were performed in June 2016. Sound velocity measurements and rebound-hammer test were performed in February 2019. Strain and AE monitoring data used in this study were collected during one year of continuous monitoring from 14/03/2019 to 14/03/2020.

Investigation of Material Properties

Concrete Strength

Rebound-Hammer Testing. Rebound-hammer testing and sound–velocity measurement help identifying material properties onsite (Breysse 2012b). They are used to estimate the modulus of elasticity of concrete.

Fig. 2. Crêt de l'Anneau viaduct located between Neuchâtel and Travers, Switzerland. (Image by authors.)

Downloaded from ascelibrary.org by 92.106.24.211 on 06/25/21. Copyright ASCE. For personal use only; all rights reserved.

Rebounds are performed in locations spaced more than 2.5 cm apart at the middle of Span 4. The 20 best readings, which are those not greater or less than 10% of the average rebound value, are used to determine the corresponding compressive strength from the conversion curve of the user manual (Proceq SA 2017). The conversion curve is chosen based on the impact direction of the rebound-hammer that forms an angle of −90°C with the tested surface. The median of the compressive strength values is then calculated and used along with the equation of the FIB model (fib 2010) to determine Young's modulus of concrete. The compressive strength is found to be equal to 47 N/mm^2 and the initial Young's modulus is taken to be approximately 35,000 N/mm^2. The actual Young's modulus is therefore found equal to 62,000 N/mm^2, which indicates a significant increase with concrete age due to the continuity of concrete hydration.

Sound–Velocity Measurement. Sound–velocity measurement is performed to obtain a second estimation of the modulus of elasticity. Elastic-wave simulations are performed using pencil-lead break and rebound-hammer testing in the middle of Span 4. Time difference Δt_1, which is given by the acquisition system in real-time for each channel is recorded. A thorough analysis of the generated waves allows for the separation of *P*-waves from *S*-waves. The time difference Δt_2 between the two wave types is calculated. The two-time differences are used along with the distance d between channels to estimate the velocity of *P*-waves and *S*-waves according to the following equations:

$$v_s = \frac{d}{\Delta t_1 + \Delta t_2} \tag{10}$$

$$v_p = \frac{d}{\Delta t_1} \tag{11}$$

Velocity results are presented in Table 2.

The density of concrete was assumed to be 2,400 kg/m^3 with a Poisson's ratio of 0.2. Young's modulus of concrete was calculated according to Eqs. (1) and (2) and was estimated to be in the range [23,000, 33,000 N/mm^2].

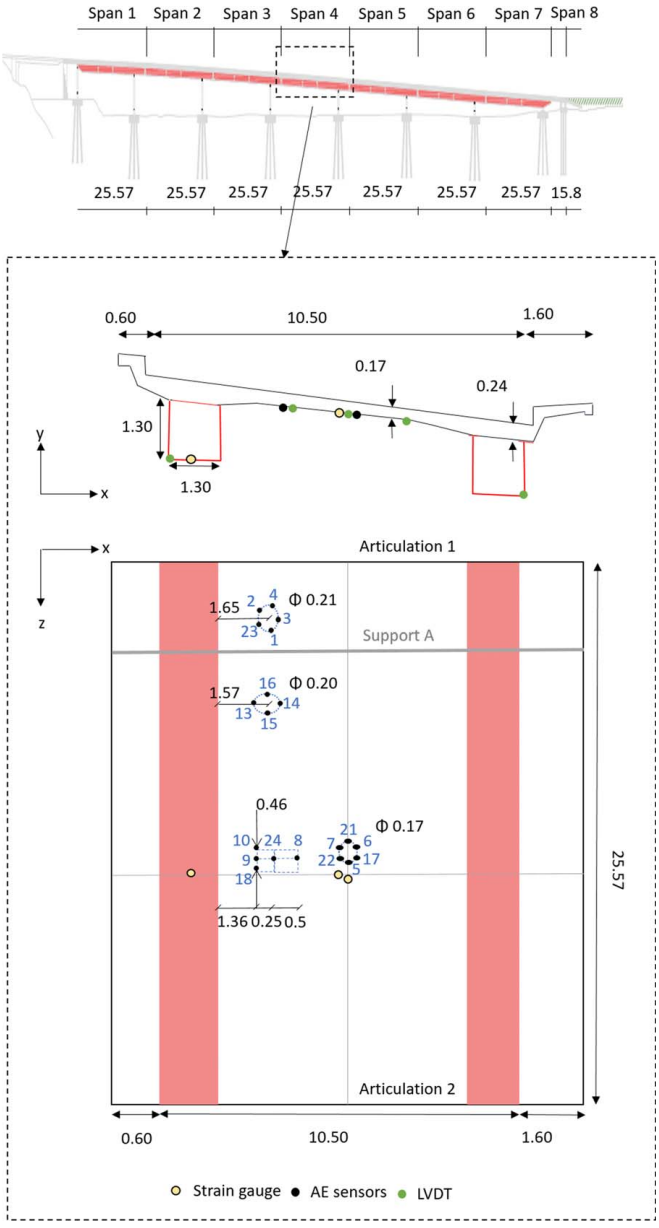

Fig. 3. Drawings of the Crêt de l'Anneau viaduct, the cross section, and the lower side of the instrumented span with sensor deployment, with dimensions in meters.

Discussion

The difference between Young's modulus of concrete obtained using rebound-hammer testing (62,000 N/mm^2) and the ones obtained using sound–velocity measurement ([23,000, 33,000] N/mm^2) is high and can be due to different factors. The validity of the values obtained is thus questionable. Factors such as the influence of the aggregate size, the influence of rebars, the humidity of concrete, the configuration of channels, the mode of propagation, or the area of investigation can all influence the results (Breysse 2012b). For example, rebound measurements have large-scale variability onsite and can give values up to 23% (Masi and Vona 2009).

The results put into question the validity of using only these measurements to estimate Young's modulus. The variability of measurement results is accommodated by making Young's modulus of concrete a parameter and varying it in the range of [20,000, 60,000] N/mm^2, as defined by the minimum and maximum values obtained with rebound-hammer testing and sound–velocity measurement.

Homogeneity of Concrete

Parametric-Based Analysis

The homogeneity of concrete is evaluated using the AE data of five channels covering different zones of the RC slab. Five classes are defined, presenting the AE data of Channel 1 near Support A, Channel 14 near Articulation 1, Channel 21 at the midspan, Channel 8 near the midlane, and Channel 24 at the midlane (see Fig. 3 for channel placement).

The classes are visualized in Fig. 4. Each point on the scatterplot represents the daily mean of an AE feature and the point marker shows the class to which the point belongs. The two dimensions of visualization present AE features for which the ABSenergy and amplitude provide information on the intensity of internal changes, while duration and Ifrequency characterize their nature

Table 2. Sound–velocity measurements

Elastic-wave simulation method	Area of interest (m)	v_p (m/s)	v_s (m/s)
Pencil-lead break	0.04	3,400	2,400
Rebound-hammer	2	3,500	2,000

Downloaded from ascelibrary.org by 92.106.24.211 on 06/25/21. Copyright ASCE. For personal use only; all rights reserved.

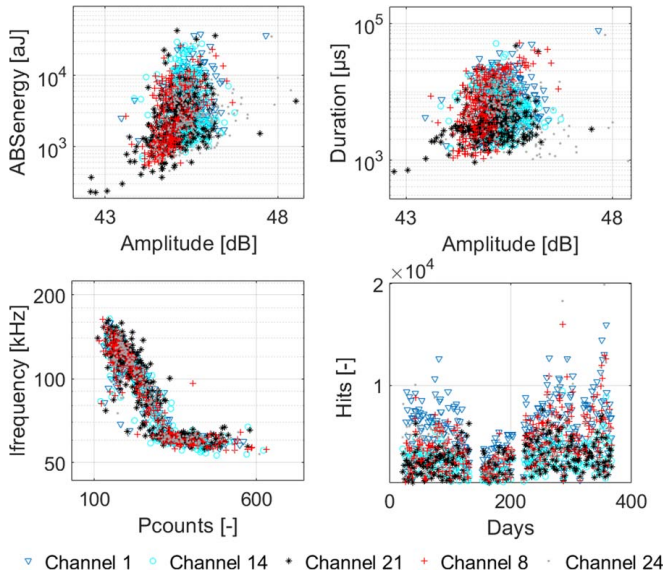

Fig. 4. Daily mean variation of acoustic emission features for Channels 1, 14, 21, 8, and 24 covering different zones of the reinforced concrete slab.

(cracking, friction, and so on). In addition, the number of hits can indicate the presence of cracking activity.

The AE activity of the channels distributed along the RC slab is grouped in one cluster for different combinations of AE features that present the dimensions of visualization. First, the daily mean of ABSenergy plotted against amplitude forms one cluster for the five channels, which implies that the detected intensity of AE activity is the same for Channels 1, 14, 21, 8, and 24. Moreover, daily mean values of Ifrequency plotted against Pcounts and duration plotted against amplitude form one cluster for the five channels, which imply that the principal source of AE activity is the same for concrete around the channels in question. The number of hits over time is also similar for the five channels, which indicates similar cracking activity in the concrete.

It is concluded that the AE response of the five channels classified in one cluster implies similar internal changes in the concrete near these channels. Concrete is therefore estimated to be homogenous along the slab for the development of the structural models.

Ib-Value Analysis

The cracking activity in the slab due to passing vehicles and environmental influence is evaluated using *Ib*-value analysis. *Ib*-value is calculated for five Channels 1, 14, 21, 8, and 24 using a step of 1,500 AE hits according to Eq. (5). Table 3 illustrates the variation in *Ib*-values.

The annual range of *Ib* value is between 1.2 and 2.5, which indicates that 48% of AE activity is due to stable cracks and 51% is due to the opening of microcracks.

Ib-values have the same variation range for channels at different locations. The cracking process of concrete is, therefore, considered to be the same along the slab. This provides further evidence for modeling the concrete of the slab as a homogeneous material with insignificant spatial variability.

Investigation of Structural Elements

AE features are classified into groups to better understand and compare the different sources of AE activity. The source of AE activity provides information on the condition of structural elements near

Table 3. Percentage of *Ib* values for Channels 1, 14, 21, 8, and 24

Channel	<1.2 (%)	<1.2–1.7> (%)	>1.7 (%)
Channel 1	1	48	51
Channel 14	1	51	48
Channel 21	1	47	51
Channel 8	0	43	57
Channel 24	1	48	51

Note: See Fig. 4 for channel placement.

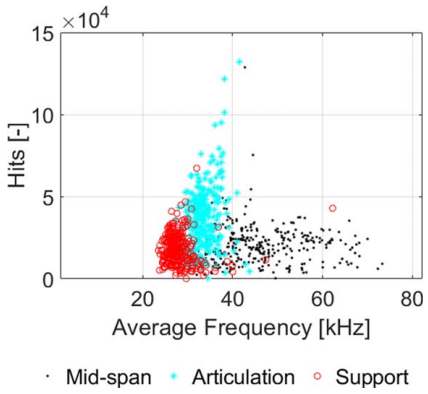

Fig. 5. Hits versus AF for channels at the midspan, and near the articulation, and near the support.

the AE channels, i.e., the condition of the support and articulation and the condition of the connection slab–girder.

Conditions of the Support and Articulation

To evaluate the condition of the support and articulation and the condition of the connection slab–girder, three classes of AE response are defined: the AE data of channels at the midspan (Channels 5, 6, 7, 17, 21, and 22), and the AE data of channels near the connection slab–girder, that are near Articulation 1 (Channels 2, 3, and 4) and near Support A (Channels 1, 16, and 23).

These classes are visualized in Fig. 5. Each point on the scatterplot represents the daily mean of the number of hits plotted against AF and the point marker shows the class to which each point belongs. The AF is calculated for each grid of channels using Eq. (3).

The daily mean of the number of hits plotted against AF forms three clusters for the three defined classes. AE response of channels near Support A and Articulation 1 present lower values of AF and a higher number of hits compared to channels at midspan, which is due to the existence of different AE sources.

The clusters with a high number of hits (>3,000) or low values of AF (<40 kHz) suggest the existence of many AE events with a long duration that are assumed to be due to friction at the level of structural elements rather than internal changes in the concrete. More details can be found in Bayane and Brühwiler (2020).

It is concluded that the three defined clusters of the AE response imply the presence of different sources of AE near the channels in question. The sources are estimated to be due to microcracking in concrete and to friction at the level of the connection slab–girder, friction at the level of articulation, and friction at the level of support. The degrees of stiffness of the support and articulation and the connection slab–girder are therefore parametrized in the development of the structural models.

Condition of the Slab–Girder Connection

The condition of the slab–girder connection is evaluated using the AE data of three grids of channels covering different zones of the

Downloaded from ascelibrary.org by 92.106.24.211 on 06/25/21. Copyright ASCE. For personal use only; all rights reserved.

RC slab near the connection slab–girder. Three classes are defined to present the AE data of Grid 1, which includes Channels 9, 10, and 18; Grid 2, which includes Channel 13; and Grid 3, which includes Channels 2 and 23 (see Fig. 3 for channel placement).

The classes are visualized in Fig. 6. Each point on the scatterplot represents the daily mean of an AE feature and the point marker shows the class to which the point belongs. The two dimensions of visualization present the ABSenergy and amplitude, which provide information on the intensity of internal changes, and the duration and Ifrequency that characterize the nature of internal changes.

The daily mean of ABSenergy values plotted against AF, duration plotted against amplitude, and Pcount plotted against Ifrequency form one cluster for the three grids of channels, which implies that the intensity and the source of internal changes are the same for channels near the connection slab–girder.

The three defined classes of AE response form one cluster, which implies that the condition of the slab–girder connection is stable along the bridge deck. The stiffness of the slab–girder connection is therefore considered constant throughout the span during the development of structural models.

Investigation of Structural Response

During the load test, strain responses are measured in the longitudinal rebars at the middle of Span 4 using strain gauges. Moreover, the maximum deflection of the cross section is measured using LVDTs. The load-test results are used to update the numerical model and assess the condition of the slab–girder connection.

The truck is driven along the center of the bridge at an approximate velocity of 10 km/h. During the load test, the truck was stopped for 10 s in the middle of the span. The passage of the five-axle truck generates five peaks in the longitudinal strain. Moreover, the stress reversal is present in the longitudinal response. The response of the slab on the passage of the load-test truck is used to compare simulation and measurement results. The comparison is made in the next section.

Model-Based Data Interpretation

Finite-Element Model

Model updating enables the development of physics-based models of the viaduct that can accurately simulate its behavior under conditions that are different from those present during monitoring. The model is developed based on the prior knowledge provided by AE measurements. The slab is modeled as homogenous because the variability of AE features across the slab is similar. The Young's modulus value is parametrized to be uniformly distributed in the range [20,000, 60,000] N/mm^2, which is defined according to the minimum and maximum values obtained with rebound-hammer testing and sound–velocity measurement. Springs are introduced between the slab and the girder to parametrize the stiffness of the slab–girder connection due to the existence of friction between the slab and the girder, detected by AE activity. Spring stiffness is constant across the slab since the AE features of channels near the connection present the same variation at all locations. The stiffness of supports and articulations is parametrized because of the existence of friction at their level, as detected by AE activity.

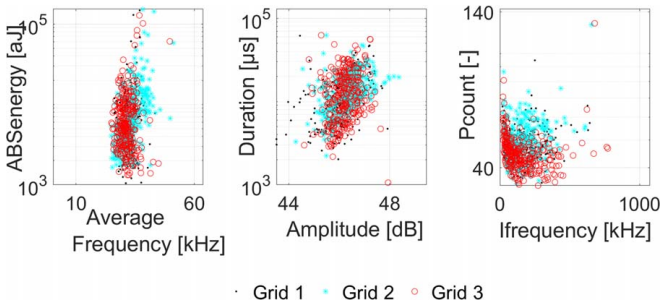

Fig. 6. Daily mean variation of AE features for channels near the slab–girder connection.

The noninstrumented spans of the viaduct are independent and assumed to have similar structural behavior compared to Span 4. The model is therefore comprised of one span, modeled from articulation to articulation. The FEM of the viaduct is developed using ANSYS R18 (a commercial program). Material properties and boundary condition properties are presented in Tables 4 and 5. The RC slab and the girder are modeled using Shell Element 181. The support, articulation, and connection slab–girder are modeled using zero-length spring elements, Combin 14, to parametrize their translational and rotational stiffness. The ranges of possible model parameters are presented in Table 6.

The parameter range is defined based on structural response variations depending on spring stiffness. The structural response variation has an *S* shape in which the initial range of parameters is defined for the variable part. The first part of the constant values corresponds to the lack of stiffness and the last part of the constant

Table 4. Material properties

Material	Density (kN/m^3)	Young's modulus (N/mm^2)	Poisson's ratio	Element
Reinforced concrete (slab)	25	Variable in the range [20,000, 60,000]	0.2	Shell 181
Steel (girder)	78.5	210,000	0.3	Shell 181

Table 5. Boundary condition properties

Boundary condition	Stiffness[a]	Element
Articulation	Variable	Combin 14
Support	Variable	Combin 14
Connection slab–girder	Variable	Combin 14

[a]See Table 6 for the range of the variable.

Table 6. Range of model parameters

Parameter	Description	Initial range
E_c	Young's modulus of concrete (N/mm^2)	20,000–60,000
K_{sg_x}	Stiffness of the connection slab–girder *x*-direction (log N/mm)	3–9
K_{sg_z}	Stiffness of the connection slab–girder *z*-direction (log N/mm)	4–8
K_{sup_y}	Stiffness of the support *y*-direction (log N/mm)	3–7
K_{sup_z}	Stiffness of the support *z*-direction (log N/mm)	4–9
R_{sup_x}	Stiffness of the support *x*-direction (log N/mm)	7–12
K_{art1_y}	Stiffness of the Articulation 1 *y*-direction (log N/mm)	2–6
K_{art1_z}	Stiffness of the Articulation 2 *z*-direction (log N/mm)	4–8
K_{art2_y}	Stiffness of the Articulation 2 *y*-direction (log N/mm)	2–6
K_{art2_z}	Stiffness of the Articulation 2 *z*-direction (log N/mm)	4–8

Downloaded from ascelibrary.org by 92.106.24.211 on 06/25/21. Copyright ASCE. For personal use only; all rights reserved.

values presents full stiffness. For example, in Fig. 7, the strain variation ε_L of the longitudinal rebar at the midspan is S-shaped when changing the stiffness of the connection slab–girder K_{sg_z}. The initial range of the parameter K_{sg_z} is therefore defined as [4, 8].

In Fig. 8, a comparison between simulations and measurements is shown. In the figure, the comparison is made between the influence lines obtained as the truck moves across the bridge. The five-axle truck crosses the span with a velocity of approximately 10 km/h. The axle loads are moved along the span to obtain the influence line for the truck. Comparisons between measured and simulated strains and deflections are presented in Fig. 8. Measurements are converted from time scale to distance scale using truck speed to facilitate comparison.

The similarity between the model response and measurements suggests that the model adequately describes the influence lines of the five-axle truck. The influence lines of deflection and strain obtained using the model are similar to the influence lines of deflection and strain measured during the load test. Variability of results using the model and measurements are likely due to modeling imperfections as well as small changes in the truck velocity during the load test (approximated to a constant value of 10 km/h).

Model Class Selection

The FEM of the viaduct is used to predict strain distribution and deflection at each sensor location. Strain and deflection are affected differently by the parameters that define the model. Each model parameter is quantified as a random variable with a uniform probability distribution. Bounds of the uniform probability distribution

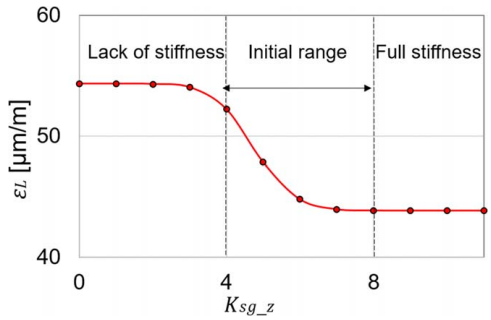

Fig. 7. Variation of the strain of the longitudinal rebar at the midspan based on spring stiffness; the variation of the structural response to spring stiffness forms an *S* shape.

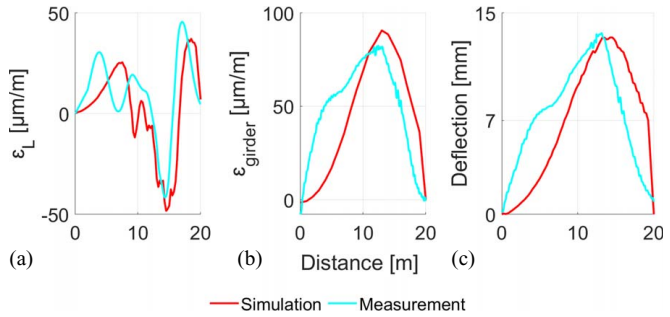

Fig. 8. Comparison of the numerical simulation and measurements of influence lines due to the passage of the load-test truck approximately at 10 km/h at the middle of the span: (a) longitudinal strain; (b) strain in the girder; and (c) deflection.

attributed to the parameters are updated using deflection measurements.

A total of 10 parameters are included in the FEM. The model class for structural identification is selected using forward-variable selection to search for a globally relevant model class (Pai et al. 2020). One thousand random samples are drawn from the initial parameter distribution (Table 6) and are provided as inputs to the FEM to predict deflection at the five sensor locations. Clustering with *k*-means is used to characterize model predictions into classes. A support vector machine classifier model (Cristianini and Shawe-Taylor 2000) is trained using these different classes and forward-variable selection to determine parameters that govern the structural behavior. Parameters that make significant changes to predictions at measurement locations are more important for classification than others are and they are included therefore in the model class for structural identification. Five parameters out of ten are included in the model class for structural identification using this method, which are listed in Table 7.

Sources of Uncertainty

Uncertainty affecting structural identification arises from assumptions made during model development. Sources of uncertainty, such as the geometry of the RC slab and the modeling of the supports and connections between the RC slab and steel girders are important. Additional sources of uncertainty related to sensors and loading conditions are accounted for during structural identification. Uncertainties from sources such as truck position and secondary parameters are estimated by varying these as parameters in the FEM. Uncertainties due to modeling assumptions are estimated based on engineering heuristics. Uncertainties in measurements are estimated either using the technical manual provided by sensor manufacturers or by comparing measurements recorded during multiple load tests. Table 8 shows the estimated distributions of uncertainties from different modeling sources. Table 9 shows the

Table 7. Ranges of prior parameter distribution

	Parameter	Description	Range
1	K_{sg_z}	Stiffness of the connection slab–girder *z*-direction (log N/mm)	4–8
2	K_{sup_y}	Stiffness of the support *y*-direction (log N/mm)	3–7
3	K_{sup_z}	Stiffness of the support *z*-direction (log N/mm)	4–9
4	K_{art1_y}	Stiffness of the Articulation 1 *y*-direction (log N/mm)	2–6
5	K_{art1_z}	Stiffness of the Articulation 1 *z*-direction (log N/mm)	4–8

Table 8. Uncertainty sources and distribution (other than measurement)

Source	Min	Max	Distribution
Model	−10%	5%	Uniform
Position	>−6%	0	Uniform
Load	0	10^{-3}	Uniform
Secondary parameters	>−12%	<15%	Uniform

Table 9. Uncertainty sources and distribution (measurement)

Sensor	Mean	Standard deviation	Distribution
Strain gauge	0	1 μm/m	Normal
LVDT	0	1 mm	Normal

Downloaded from ascelibrary.org by 92.106.24.211 on 06/25/21. Copyright ASCE. For personal use only; all rights reserved.

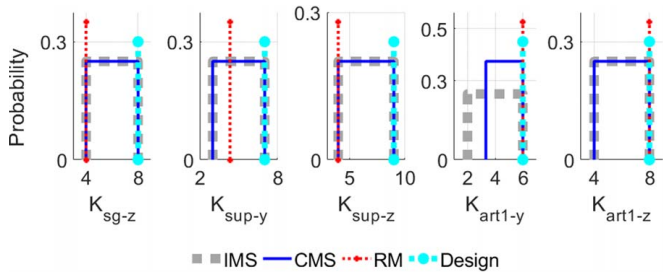

Fig. 9. Probability of the bounds of IMS, CMS, RM solutions, and initial design values (design).

estimation of measurement uncertainty distributions related to strain gauges and LVDTs.

The most important uncertainty sources do not have a zero mean. Uncertainties defined in Tables 8 and 9 are combined using Monte Carlo sampling to estimate the combined uncertainty at each sensor location. Using this combined uncertainty, threshold bounds for EDMF are calculated for each sensor location using Eq. (6). The threshold bounds are calculated for target reliability of identification of 0.95 (95% confidence). These bounds are used to perform EDMF using the condition defined in Eq. (8).

Structural Identification Using Load-Test Data

EDMF is used to update the FEM of the steel–concrete composite viaduct with information from measurement data recorded during the load test. RM that assumes no model bias is also used to calculate the optimal solution using Eq. (9). Five measurement data points are utilized for structural identification, which are midspan deflections at five locations in the cross section. The location of LVDT sensors for measuring deflection is shown in Fig. 3.

Grid-based sampling is used to generate the parameter space. The five identification parameters are discretized in four uniform intervals, giving $4^5 = 1{,}024$ samples. EDMF identifies 165 candidates in the CMS from an IMS of 1,024 samples. The identified candidates in the CMS reduce the initial uncertainty related to model parameter values in the IMS and provide predictions that are compatible with measurements. On the other hand, RM identifies one solution without considering measurement uncertainties, thereby assuming that either there is no uncertainty or that the total uncertainty has a zero mean and that there are a statistically significant number of measurements.

In Fig. 9, the probability of the bounds of the IMS and EDMF solutions that form the CMS are shown. Furthermore, parameter values obtained using RM and design parameter values (design) are shown.

The updated model instances obtained using EDMF reduces variability related to the stiffness of Articulation 1 in the y-direction, which means that the translational stiffness of the articulation in the y-direction cannot be free. While the probabilities of Parameters 1, 2, 3, and 5 have similar bounds to the prior parameter ranges, the parameter variability related to the joint model parameter probability is reduced as demonstrated by the falsification of 84% of initial model instances. A parallel axis plot comparing the initial model population with the CMS identified using EDMF is shown in Fig. 10.

Each point along these vertical axes corresponds to a possible value of the five chosen parameters. The bounds of the vertical axis denoted as minimum and maximum correspond to the bounds of prior parameter distributions presented in Table 6.

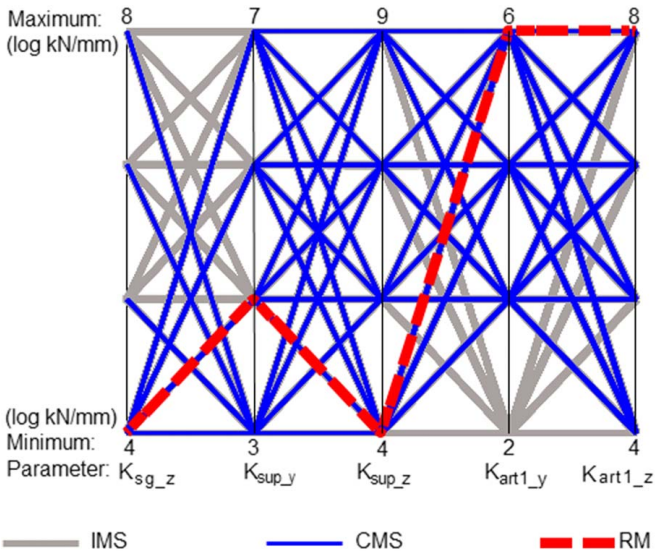

Fig. 10. Parallel axis plot comparing IMS, CMS, and the optimal solution obtained using RM.

Therefore, a line connecting minimum values represents a model instance with the following input parameters:

$$K_{sg\_z} = 4,\ K_{\text{sup}\_y} = 3,\ K_{\text{sup}\_z} = 4,\ K_{\text{art1}\_y} = 2 \text{ and } K_{\text{art1}\_z} = 4$$

A line connecting maximum values represents a model instance with the following input parameters:

$$K_{sg\_z} = 8,\ K_{\text{sup}\_y} = 7,\ K_{\text{sup}\_z} = 9,\ K_{\text{art1}\_y} = 6 \text{ and } K_{\text{art1}\_z} = 8$$

The possible combinations of model–parameter values that provide predictions compatible with measurements (as assessed by EDMF and illustrated by the CMS line, Fig. 10) form the CMS. This CMS consists of 16% of the initial model instances.

The optimal parameter values obtained using RM are also shown in Fig. 10. RM solution indicates stiff articulation, flexible support, and lack of stiffness between the slab and the girder. This solution is far from the most conservative solution identified by EDMF.

While Fig. 10 helps visualize a multidimensional parameter space, it does not provide information related to the accuracy of data interpretation. The next section describes data-interpretation solutions that have been validated with additional data that has not been utilized in model-based data interpretation.

Validation

Strain measurements are used to validate solutions of structural identification that are obtained using EDMF and RM. Validation is carried out using measurements from strain gauges in the longitudinal rebar ε_L and the steel girder $\varepsilon_{\text{girder}}$ at the midspan. Updated-model parameters are used to predict the strain at these sensor locations. A comparison of the predicted and measured strains for the two sensors is shown in Fig. 11.

The range of predicted strain is lower than the initial prediction range due to model falsification, which reduces parameter variability. The bounds of the updated-model prediction distributions include measurements from all sensors excluded from structural identification. The results are therefore assumed to be accurate, and the updated model parameters can be used to predict conservative model responses at nonaccessible locations.

Downloaded from ascelibrary.org by 92.106.24.211 on 06/25/21. Copyright ASCE. For personal use only; all rights reserved.

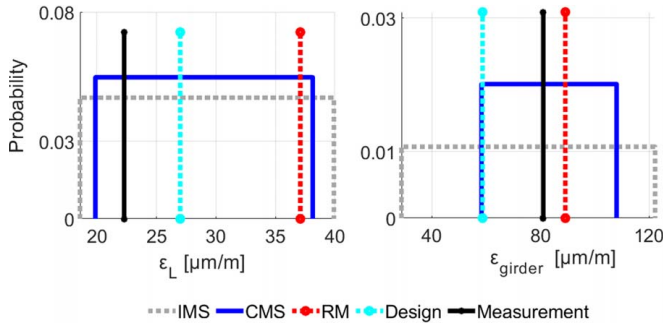

Fig. 11. Validation results, comparison of the predicted and measured strains that have been left out of identification. CMS bounds include measurements, which validate structural identification predictions while RM fails to predict measurements that are far away from the RM solution.

RM predictions of strain are biased from measurements, despite calibrating parameter values with deflection measurements. The RM solution is therefore not valid and may result in unconservative predictions.

Fatigue Evaluation

The cross section of the RC slab is defined as the critical element of the viaduct due to the pronounced effect of axle loads. In fact, in the longitudinal direction, traffic loads are distributed on both the RC slab and the steel girder. While in the transverse direction, only the 17-cm-thickness slab is acting. Therefore, the fatigue behavior of steel reinforcement and concrete of the cross section are evaluated with respect to fatigue requirements. Details of fatigue damage calculation can be found in Bayane et al. (2019) and Bayane and Brühwiler (2018).

The RC slab is found to be safe considering the combined action of the slab and the girder under traffic loading. However, the flexural behavior of the cross section depends on the capacity of the welded rebars to ensure the fixity between the slab and the girder. The welded rebars are used to connect the steel girder and the slab and they are not accessible for monitoring, as illustrated in Fig. 12.

Welded rebars are therefore considered a critical fatigue detail. The fatigue resistance of the welded rebars is equal to 70 MPa, and their endurance limit is equal to 80% of the constant-amplitude fatigue limit, which is 56 MPa according to SIA 269 (SIA 2013b). Influence lines of the welded rebar at the midspan are calculated using the 165 candidate model instances. Calculations are performed using the load model described in SIA 262 (SIA 2013a) and SIA 269 (SIA 2013b).

The maximum stress range is found to be equal to 12 MPa, which is four times less than the fatigue limit. The fatigue evaluation is therefore fulfilled, and no fatigue problem is detected for the welded rebars.

Influence lines of the welded rebar are calculated using parameter values obtained from RM by applying the same load model. The maximum stress range is found equal to 14 MPa, which is below the fatigue limit. RM solutions do not pass the validation test even though they lead to the same conclusion of there being no fatigue problem. Therefore, predictions with RM are inaccurate and cannot be used for decision-making.

The welded rebars are assessed as safe using monitoring and model-based interpretations. The RC slab is therefore safe with respect to the fatigue limit state even though it is not designed against fatigue. This evaluation adds to the growing body of evidence that most existing concrete bridges do not risk exceeding the fatigue limit state under traffic loading, while they are not explicitly designed against fatigue (Fehlmann 2012; SIA 1997; Siemes and TNO Institue for building materials and structures 1988). Quantifying RC slab safety can enable better asset-management decision-making when, for example, loading increases, codes change, or deterioration occurs.

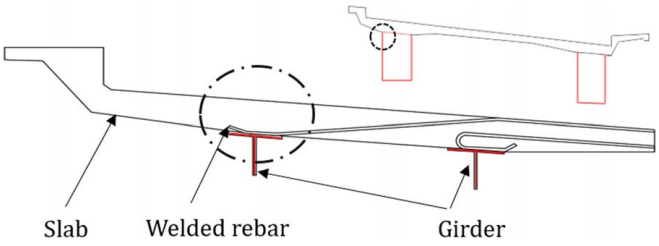

Fig. 12. Details of welded rebars.

Conclusions

The proposed methodology utilizes monitoring data from many sources to develop accurate physics-based models for evaluating the fatigue of existing infrastructure. The following conclusions can be drawn from this study:

- Prior to load testing, data from AE and NDT estimates information related to material properties and structural element conditions and assist in the development of an accurate set of models for bridge examination.
- Using physics-based models and EDMF to interpret measurements enables the accurate identification of structural parameters and prognoses regarding the structural safety and performance evaluations of structural elements that cannot be directly instrumented.
- RM provides inaccurate structural identification and may not lead to conservative predictions due to inaccurate assumptions related to modeling uncertainty and bias.
- For the Crêt de l'Anneau viaduct, stress ranges predicted for design loads are small, which indicates that fatigue limits are not exceeded. Hence, the bridge is safe with respect to the fatigue limit state.
- Using monitoring data, the slab–girder connection is assessed to be safe, despite a difference between the present condition and the design assumptions. This adds to the growing body of evidence that most structural elements are safer than design requirements. It is expected that quantifying their safety will enable better asset-management decision-making in many situations.

Data Availability Statement

All data, models, and codes that support the findings of this study are available from the corresponding author upon reasonable request.

Acknowledgments

This research work was performed within the European project INFRASTAR (infrastar.eu), which has received funding from the

Downloaded from ascelibrary.org by 92.106.24.211 on 06/25/21. Copyright ASCE. For personal use only; all rights reserved.

European Union's Horizon 2020 research and innovation program under the Marie Skłodowska-Curie Grant Agreement No. 676139. This work was funded by the Swiss National Science Foundation under Contract No. 200020-169026 and the Singapore-ETH Centre (SEC) under Contract No. FI 370074011-370074016. These grants are gratefully acknowledged.

References

AFNOR (Association Française de Normalisation). 2013. *Testing concrete in structures—Part 2: Non-destructive testing—Determination of rebound number*. NF EN 12504-2. Paris: AFNOR.

Aggelis, D. G. 2011. "Classification of cracking mode in concrete by acoustic emission parameters." *Mech. Res. Commun.* 38 (3): 153–157. https://doi.org/10.1016/j.mechrescom.2011.03.007.

Anay, R., T. M. Cortez, D. V. Jáuregui, M. K. ElBatanouny, and P. Ziehl. 2016. "On-site acoustic-emission monitoring for assessment of a prestressed concrete double-tee-beam bridge without plans." *J. Perform. Constr. Facil* 30 (4): 04015062. https://doi.org/10.1061/(ASCE)CF.1943-5509.0000810.

Bayane, I., and E. Brühwiler. 2018."'Pocket-Monitoring' for fatigue safety verification of a RC bridge deck slab." In *Proc., 6th Int. Symp. on Life-Cycle Civil Engineering*, 1–8. Boca Raton, FL: CRC Press.

Bayane, I., and E. Brühwiler. 2020. "Structural condition assessment of reinforced-concrete bridges based on acoustic emission and strain measurements." *J. Civ. Struct. Health Monit.* 10 (5): 1037–1055. https://doi.org/10.1007/s13349-020-00433-0.

Bayane, I., A. Mankar, E. Brühwiler, and J. D. Sørensen. 2019. "Quantification of traffic and temperature effects on the fatigue safety of a reinforced-concrete bridge deck based on monitoring data." *Eng. Struct.* 196: 109357. https://doi.org/10.1016/j.engstruct.2019.109357.

Beattie, A. G. 2013. *Acoustic emission non-destructive testing of structures using source location techniques*. Livermore, CA: Sandia National Laboratories.

Breysse, D. 2012a. *Non-destructive assessment of concrete structures: Reliability and limits of single and combined techniques: State-of-the-art report of the RILEM technical committee 207-INR*. Berlin: Springer.

Breysse, D. 2012b. "Nondestructive evaluation of concrete strength: An historical review and a new perspective by combining NDT methods." *Constr. Build. Mater.* 33: 139–163. https://doi.org/10.1016/j.conbuildmat.2011.12.103.

Carpinteri, A., G. Lacidogna, and S. Puzzi. 2009. "From criticality to final collapse: Evolution of the '*b*-value' from 1.5 to 1.0." *Chaos Solitons Fractals* 41 (2): 843–853. https://doi.org/10.1016/j.chaos.2008.04.010.

Colombo, I. S., I. G. Main, and M. C. Forde. 2003. "Assessing damage of reinforced concrete beam using '*b*-value' analysis of acoustic emission signals." *J. Mater. Civ. Eng.* 15 (3): 280–286. https://doi.org/10.1061/(ASCE)0899-1561(2003)15:3(280).

Cristianini, N., and J. Shawe-Taylor. 2000. *An introduction to support vector machines and other kernel-based learning methods*. Cambridge, UK: Cambridge University Press.

Farrar, C. R., and K. Worden. 2010. "An introduction to structural health monitoring." In *New trends in vibration based structural health monitoring, CISM courses and lectures*, edited by A. Deraemaeker and K. Worden, 1–17. Vienna, Austria: Springer.

Fehlmann, P. 2012. *Zur Ermüdung von Stahlbetonbrücken*. Zürich, Switzerland: ETH Zurich.

Felux, M. W. 2017. "Acoustic emission monitoring on bridges under regular operating conditions." Thesis, ETH Zurich.

fib (International Federation for Structural Concrete). 2010. *Fib model code for concrete structures 2010*. Lausanne, Switzerland: fib.

Golaski, L., P. Gebski, and K. Ono. 2002. "Diagnostics of reinforced concrete bridges by acoustic emission." *J. Acous. Emission* 20: 83–89.

Goulet, J.-A., and I. F. C. Smith. 2013. "Structural identification with systematic errors and unknown uncertainty dependencies." *Comput. Struct.* 128: 251–258. https://doi.org/10.1016/j.compstruc.2013.07.009.

Maierhofer, C., H.-W. Reinhardt, and G. Dobmann. 2010. *Non-destructive evaluation of reinforced concrete structures: Non-destructive testing methods*. Amsterdam, Netherlands: Elsevier.

Masi, A., and M. Vona. 2009. "La stima della resistenza del calcestruzzo in situ: Impostazione delle indagini ed elaborazione dei risultati." *Progettazione Sismica* 18 (1): 53–57.

Mauro, P. 2017. "Long-term investing, infrastructure and development." World Economic Forum. Accessed July 22, 2020. https://www.weforum.org/agenda/2017/03/before-roads-and-bridges-we-need-checks-and-balances/.

Méndez, A., and A. Csipkes. 2013. "Overview of fiber optic sensors for NDT applications." In *Nondestructive testing of materials and structures*, edited by O. Güneş and Y. Akkaya, 179–184. Dordrecht, Netherlands: Springer.

MISTRAS. 2015. *Sensor highway III, user's manual*. Princeton, NJ: MISTRAS.

Moser, G., S. G. Paal, and I. F. C. Smith. 2018. "Leak detection of water supply networks using error-domain model falsification." *J. Comput. Civil Eng.* 32 (2): 04017077. https://doi.org/10.1061/(ASCE)CP.1943-5487.0000729.

Mottershead, J. E., M. Link, and M. I. Friswell. 2011. "The sensitivity method in finite element model updating: A tutorial." *Mech. Syst. Sig. Process.* 25 (7): 2275–2296. https://doi.org/10.1016/j.ymssp.2010.10.012.

Nair, A., and C. S. Cai. 2010. "Acoustic emission monitoring of bridges: Review and case studies." *Eng. Struct.* 32 (6): 1704–1714. https://doi.org/10.1016/j.engstruct.2010.02.020.

Nguyen, N. T., Z.-M. Sbartaï, J.-F. Lataste, D. Breysse, and F. Bos. 2013. "Assessing the spatial variability of concrete structures using NDT techniques—Laboratory tests and case study." *Constr. Build. Mater.* 49: 240–250. https://doi.org/10.1016/j.conbuildmat.2013.08.011.

Pai, S. G. S., A. Nussbaumer, and I. F. C. Smith. 2018. "Comparing structural identification methodologies for fatigue life prediction of a highway bridge." *Front. Built Environ.* 3: 73. https://doi.org/10.3389/fbuil.2017.00073.

Pai, S. G. S., M. Sanayei, and I. F. C. Smith. 2020. "Model class selection using clustering and classification for structural identification and prediction." *J. Comput. Civil Eng.* 35 (1): 04020051. https://doi.org/10.1061/(ASCE)CP.1943-5487.0000932.

Pasquier, R., L. D'Angelo, J.-A. Goulet, C. Acevedo, A. Nussbaumer, and I. F. C. Smith. 2016. "Measurement, data interpretation, and uncertainty propagation for fatigue assessments of structures." *J. Bridge Eng.* 21 (5): 04015087. https://doi.org/10.1061/(ASCE)BE.1943-5592.0000861.

Pasquier, R., J.-A. Goulet, C. Acevedo, and I. F. C. Smith. 2014. "Improving fatigue evaluations of structures using in-service behavior measurement data." *J. Bridge Eng.* 19 (11): 04014045. https://doi.org/10.1061/(ASCE)BE.1943-5592.0000619.

Popper, K. 2005. *Popper-the logic of scientific discovery*. New York: Taylor & Francis.

Proceq SA. 2017. *Concrete test hammer*. Schwerzenbach, Switzerland: Proceq SA.

Proverbio, M., D. G. Vernay, and I. F. C. Smith. 2018. "Population-based structural identification for reserve-capacity assessment of existing bridges." *J. Civ. Struct. Health Monit.* 8 (3): 363–382. https://doi.org/10.1007/s13349-018-0283-6.

Reuland, Y., P. Lestuzzi, and I. F. C. Smith. 2019a. "Measurement-based support for post-earthquake assessment of buildings." *Struct. Infrastruct. Eng.* 15 (5): 647–662. https://doi.org/10.1080/15732479.2019.1569071.

Reuland, Y., P. Lestuzzi, and I. F. C. Smith. 2019b. "A model-based data-interpretation framework for post-earthquake building assessment with scarce measurement data." *Soil Dyn. Earthquake Eng.* 116: 253–263. https://doi.org/10.1016/j.soildyn.2018.10.008.

Sammonds, P. R., P. G. Meredith, S. a. F. Murrell, and I. G. Main. 1994. "Modelling the damage evolution in rock containing pore fluid by acoustic emission." In *Rock Mechanics in Petroleum Engineering*, 897–915. Richardson, TX: Society of Petroleum Engineers.

Shiotani, T. 2001. "Application of the AE improved *b*-value to quantitative evaluation of fracture processes in concrete materials." *J. Acous. Emission* 19: 118–133.

Downloaded from ascelibrary.org by 92.106.24.211 on 06/25/21. Copyright ASCE. For personal use only; all rights reserved.

SIA (Swiss Society of Engineers and Architects). 1997. *Ermüdung von Betonbauten*. SIA Dokumentation. Zurich, Switzerland: SIA.
SIA (Swiss Society of Engineers and Architects). 2013a. *Concrete structures*. SIA 262. Zurich, Switzerland: SIA.
SIA (Swiss Society of Engineers and Architects). 2013b. *Existing structures—Concrete structures*. SIA 269. Zurich, Switzerland: SIA.
Siemes, A. J. M., and TNO Institute for Building Materials and Structures. 1988. "Fatigue evaluation of concrete structures preliminary studies, procedure and examples." *HERON* 33 (3): 75.
Smith, I. F. C. 2016. "Studies of sensor data interpretation for asset management of the built environment." *Front. Built Environ.* 2: 8. https://doi.org/10.3389/fbuil.2016.00008.
Sorenson, H. W. 1970. "Least-squares estimation: From Gauss to Kalman." *IEEE Spectr.* 7 (7): 63–68. https://doi.org/10.1109/MSPEC.1970.5213471.
Vernay, D. G., F.-X. Favre, and I. F. C. Smith. 2018. "Robust model updating methodology for estimating worst-case load capacity of existing bridges." *J. Civ. Struct. Health Monit.* 8 (5): 773–790. https://doi.org/10.1007/s13349-018-0305-4.
Whitehurst, E. A. 1966. *Evaluation of concrete properties from sonic tests*. Farmington Hills, MI: American Concrete Institute.
Xu, Z. Z., Y. Wang, S. X. Wu, and Y. Wang. 2013. "Damage evaluation of concrete based on acoustic emission *b*-value." *Appl. Mech. Mater.* 395–396: 515–519. https://doi.org/10.4028/www.scientific.net/AMM.395-396.515.

Downloaded from ascelibrary.org by 92.106.24.211 on 06/25/21. Copyright ASCE. For personal use only; all rights reserved.